



HAL
open science

Universal Symmetry Breaking Dynamics for the Kerr Interaction of Counter-Propagating Light in Dielectric Ring Resonators

Michael T M Woodley, Jonathan M Silver, Lewis Hill, François Copie, Leonardo del Bino, Shuangyou Zhang, Gian-Luca Oppo, Pascal Del'Haye

► **To cite this version:**

Michael T M Woodley, Jonathan M Silver, Lewis Hill, François Copie, Leonardo del Bino, et al.. Universal Symmetry Breaking Dynamics for the Kerr Interaction of Counter-Propagating Light in Dielectric Ring Resonators. *Physical Review A*, 2018, 98 (5), 10.1103/PhysRevA.98.053863 . hal-02406849

HAL Id: hal-02406849

<https://hal.science/hal-02406849>

Submitted on 12 Dec 2019

HAL is a multi-disciplinary open access archive for the deposit and dissemination of scientific research documents, whether they are published or not. The documents may come from teaching and research institutions in France or abroad, or from public or private research centers.

L'archive ouverte pluridisciplinaire **HAL**, est destinée au dépôt et à la diffusion de documents scientifiques de niveau recherche, publiés ou non, émanant des établissements d'enseignement et de recherche français ou étrangers, des laboratoires publics ou privés.

Universal Symmetry Breaking Dynamics for the Kerr Interaction of Counter-Propagating Light in Dielectric Ring Resonators

Michael T. M. Woodley,^{1,2} Jonathan M. Silver,¹ Lewis Hill,³ François Copie,¹
 Leonardo Del Bino,^{1,2} Shuangyou Zhang,¹ Gian-Luca Oppo,³ and Pascal Del’Haye.¹
¹*National Physical Laboratory, Hampton Road, Teddington, TW11 0LW, UK,*
²*Heriot-Watt University, Edinburgh, EH14 4AS, UK, and*
³*Department of Physics, University of Strathclyde, Glasgow, G4 0NG, UK.*

Spontaneous symmetry breaking is an important concept in many areas of physics. A fundamentally simple symmetry breaking mechanism in electrodynamics occurs between counterpropagating electromagnetic waves in ring resonators, mediated by the Kerr nonlinearity. The interaction of counterpropagating light in bi-directionally pumped microresonators finds application in the realisation of optical nonreciprocity (for optical diodes), studies of \mathcal{PT} -symmetric systems, and the generation of counter-propagating solitons. Here, we present comprehensive analytical and dynamical models for the nonlinear Kerr-interaction of counter-propagating light in a dielectric ring resonator. In particular, we study discontinuous behaviour in the onset of spontaneous symmetry breaking, indicating divergent sensitivity to small external perturbations. These results can be applied to realise, for example, highly sensitive near-field or rotation sensors. We then generalise to a time-dependent model, which predicts new types of dynamical behaviour, including oscillatory regimes that could enable Kerr-nonlinearity-driven all-optical oscillators. The physics of our model can be applied to other systems featuring Kerr-type interaction between two distinct modes, such as for light of opposite circular polarisation in nonlinear resonators, which are commonly described by coupled Lugiato-Lefever equations.

Introduction.—Spontaneous symmetry breaking plays a critical role in the description of many phenomena in physics. In the case of continuous symmetries, it allows for the modelling of magnetism and superconductivity [1], as well as the generation of mass via the Higgs mechanism [2]. It also plays a prominent role in systems that exhibit discrete symmetries, which are frequently found in optics, such as time-reversal [3] and parity-time symmetries [4], as well as the interplay between two types of symmetry breaking [5]. A novel type of discrete symmetry breaking has recently been demonstrated in bi-directionally-pumped whispering-gallery microresonators [6, 7]. In this case, the symmetry violation is caused by an instability whereby, above a threshold pump power, a difference between the intracavity powers in the two counter-propagating directions leads to a splitting between their two resonant frequencies via the Kerr nonlinearity. As a result, small differences between the intracavity circulating powers are amplified. Consequently, the (parity) symmetry of the circulating optical power in the resonator spontaneously breaks. This is due to the fact that the cross-phase-modulation-induced Kerr shift between counter-propagating light waves is different to the self-phase-modulation-induced shift in unidirectional light. Interestingly, this imposes fundamental limits on the attainable power of a standing wave in a dielectric ring resonator. Fig. 1 shows a simple experimental platform for observing this symmetry breaking in a ring resonator.

The theoretical treatment of the Kerr interaction of counter-propagating light was pioneered by Kaplan and Meystre in the early 1980s, in the context of nonlinear

effects in Sagnac interferometers [8, 9]. A more complete theoretical basis for light-with-light interaction in ring resonators, and especially of symmetry breaking, is critically needed for a precise understanding of recent work on microresonator-based non-reciprocal devices such as isolators and circulators [10], as well as for the dynamics of counter-propagating solitons [11–13]. Here, we develop a generalised model that not only captures this symmetry breaking, but extends to a universal sensitivity analysis, which will be crucial for future sensing devices based on this effect, such as enhanced rotation sensors and near-field detectors. In addition, we generalise the model to the time domain, which should facilitate the creation of an all-optical oscillator.

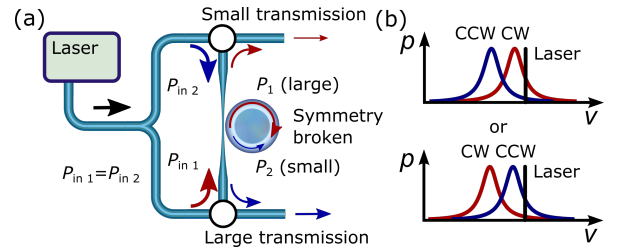


FIG. 1. A simplified schematic of a ring resonator setup in a symmetry-broken state. Amplified laser light ($\lambda = 1550$ nm) is split into two paths of equal powers, which are then sent in opposite directions into a microresonator. (b) Above a critical power threshold, the parity symmetry is broken, characterised by different resonant frequencies in the two directions, such that one direction of light is preferentially coupled into the cavity. Panel (a) shows the case for preferential coupling in the clockwise direction. CW = clockwise, CCW = counter-clockwise.

Coupled Lorentzian model.—The basis of our theory of counter-propagating light in a ring resonator is the following dimensionless model, featuring two coupled Lorentzian curves, which results from considering how the Kerr effect modifies the resonant frequency of a cavity in a non-reciprocal fashion [6]:

$$p_{1,2} = \frac{\tilde{p}_{1,2}}{1 + (p_{1,2} + 2p_{2,1} - \Delta_{1,2})^2}. \quad (1)$$

$\tilde{p}_{1,2}$ are the (dimensionless) powers of the pump laser, and $p_{1,2}$ are the powers coupled into the resonator. The apportionment of power coupled into the resonator is determined by the detuning parameters, $\Delta_{1,2}$, which are normalised to the half-linewidth of the resonance. The subscripts 1 and 2 denote clockwise and counterclockwise directions. See Ref. [14] for more information. Equations (1) are the steady-state, homogeneous solutions to a pair of coupled Lugiato-Lefever equations (see Ref. [15] for the uncoupled version). Consequently, this model extends to other nonlinear systems in which Kerr coupling occurs between two distinct modes, such as for opposite circular polarisation states [16, 17]. We now need to consider the threshold condition beyond which Eq. (1) can describe a symmetry-broken regime.

Onset of symmetry breaking.—We demonstrate here that symmetry breaking occurs only above a certain threshold pump power. We consider symmetric pumping conditions by setting $\Delta_1 = \Delta_2 = \Delta$ and $\tilde{p}_1 = \tilde{p}_2 = \tilde{p}$, and then examine the number of crossing points between the two Lorentzians, Eq. (1), in terms of $p_{1,2}$, to see where this number changes between 1 and 3 (2 stable, 1 unstable - indicative of a bistable regime, and hence symmetry breaking). Combining the two Lorentzians gives the following cubic equation:

$$[p_1 - p_2] [(p_1^2 + p_2^2 + p_1 p_2) - 2\Delta(p_1 + p_2) + \Delta^2 + 1] = 0. \quad (2)$$

The term in the first set of square brackets is the symmetric solution, whilst the rest is the symmetry-broken solution. The abrupt onset of symmetry breaking is hence described as the discontinuous intersection of a straight line with an ellipse, as shown in Fig. 2. At the points where symmetry breaking occurs, i.e., the points of intersection, $p_1 = p_2 = p_{\pm}$, the quadratic part of Eq. (2) yields

$$p_{\pm} = \frac{1}{3} \left(2\Delta \pm \sqrt{\Delta^2 - 3} \right), \quad (3)$$

for $\Delta \geq \sqrt{3}$. The p_- solution gives the coupled power at which the symmetry-broken region opens, and p_+ gives the coupled power at which it closes. Similar threshold powers apply to polarisation symmetry breaking in ring cavities, as shown in [16]. Coincidentally, Eq. (3) describes the limits of the region of bistability for the

homogeneous, steady-state solution to a Lugiato-Lefever equation for a unidirectional beam of light in a cavity [15]. The threshold power (per direction) for the same bistability in the case of a standing wave is, in fact, 3 times lower than in the unidirectional case, owing to the extra contribution from cross-phase modulation [9].

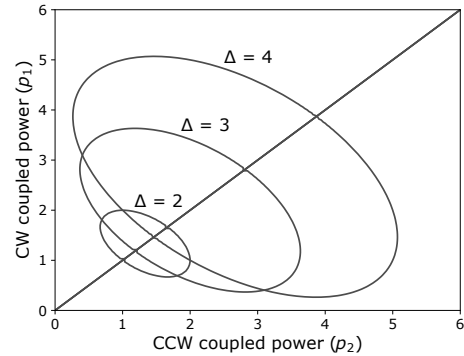


FIG. 2. Illustration of Eq. (2), each ellipse for a different (constant) value of the detuning parameter Δ . Each curve comprises all the values of $p_{1,2}$ at which the two Lorentzians, Eq. (1) intersect. When $p_1 \neq p_2$, the symmetry is broken, the threshold of which occurs where an ellipse intersects the straight line. These curves are traced out by continuously increasing the pump power, \tilde{p} .

In order to find the minimum required pump power for symmetry breaking as a function of detuning only, we first apply Eq. (3) to Eq. (1) for $p_1 = p_2 = p_{\pm}$ and $\tilde{p}_1 = \tilde{p}_2 = \tilde{p}$, to recover the equation found in [9]:

$$\tilde{p}_{\pm} = \frac{2}{3} \left[\Delta(3\Delta^2 - 5) \pm (3\Delta^2 - 1)\sqrt{\Delta^2 - 3} \right] \quad (4)$$

As for the coupled power, \tilde{p}_- gives the pump power at which the symmetry-broken region opens, and \tilde{p}_+ is where it closes. The threshold pump power is then trivially found to be

$$\tilde{p}_{\text{thresh.}} = \tilde{p}_- \left(\Delta = \frac{5}{\sqrt{3}} \right) = \frac{8}{3\sqrt{3}} \approx 1.54, \quad (5)$$

associated with the coupled power of $p = 2/\sqrt{3} \approx 1.15$.

Nonlinear enhancement of sensitivity.—We have so far considered balanced pump powers and equal detunings in both directions of propagation, in order to investigate symmetry breaking. We now consider the most general case of Eq. (1), for $\tilde{p}_1 \neq \tilde{p}_2$ and $\Delta_1 \neq \Delta_2$. The latter may be caused by using the resonator as a sensor, whereby a change in the local environment around the resonator perturbs its optical modes [18, 19], for example by inducing a small resonant frequency splitting. This can come from rotating the resonator (Sagnac effect) or from interacting with its evanescent field. This splitting can then be magnified by the Kerr nonlinearity, allowing for

enhancement of the sensitivity, theoretically down to the shot noise limit.

Divergent sensitivity.—Sensitivity, in this context, is defined as the rate of change of the coupled power with respect to the detuning. These partial derivatives are calculated to be

$$\frac{\partial p_{1,2}}{\partial \Delta_{1,2}} = \frac{(1 + X_{2,1})}{(1 + X_1)(1 + X_2) - 4}, \quad (6)$$

$$\frac{\partial p_1}{\partial \Delta_2} = \frac{\partial p_2}{\partial \Delta_1} = -\frac{2}{(1 + X_1)(1 + X_2) - 4}, \quad (7)$$

wherein

$$X_{1,2} = \frac{1 + (p_{1,2} + 2p_{2,1} - \Delta_{1,2})^2}{2p_{1,2}(p_{1,2} + 2p_{2,1} - \Delta_{1,2})}. \quad (8)$$

See Ref. [14] for more details. By inspection, the sensitivity diverges for

$$(1 + X_1)(1 + X_2) = 4. \quad (9)$$

Eq. (9) is the universal condition for maximally-enhanced sensitivity to a small perturbation to the resonator; it defines a closed boundary within the symmetry-broken regime, and is illustrated in Fig. 3. As will be demonstrated later, this condition defines the onset of instability in the system. For given pump and circulating powers, this condition defines the detunings for which sensitivity diverges. However, since the region enclosed by this boundary is unstable (see the stability analysis that follows), we find that only one particular point on this boundary is useful for nonlinear enhancement of a sensor, referred to as the critical point.

Critical point.—We view the critical point as the generalisation of the discontinuous point of symmetry breaking to the regime of imbalanced pumping conditions, in which there is no symmetry to break in the first place. This point sits on the unstable boundary, shown in Fig. 3, and is defined by the condition $X_1 = X_2 = 1$. Informally, this can be thought of as the condition that causes the sensitivity of the clockwise and counterclockwise coupled powers to diverge at equal and opposite rates. In the symmetric case, i.e., for $\tilde{p}_x = \tilde{p}_y = \tilde{p}$, $\Delta_x = \Delta_y = \Delta$, and $p_x = p_y = p$, this constraint allows us to recover the original condition for symmetry breaking, Eq. (3). Consequently, divergent sensitivity to perturbations can be accessed even in the case of imbalanced pump powers and unequal detunings. We have numerically verified this condition for the critical point. We note that the sensitivity to changes in the pump powers also diverges for this same critical point condition.

Generalisation to a time-dependent system.—We observe that the coupled Lorentzians in Eq. (1) are, in fact,

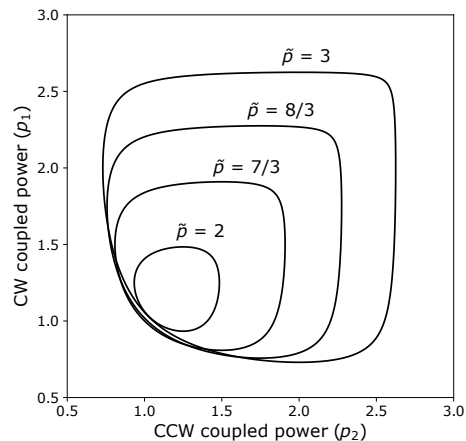


FIG. 3. Illustration of Eq. (9), in the case of balanced pump powers, $\tilde{p}_1 = \tilde{p}_2 = \tilde{p}$. Each curve corresponds to a different choice of pump powers. Each pair of circulating powers (p_1, p_2) , corresponds to a particular pair of detunings (Δ_1, Δ_2) .

the steady-state solutions to a pair of time-dependent coupled mode equations. We introduce the ‘normalised electric fields’: $p_1 = |e_1|^2$, $p_2 = |e_2|^2$, $\tilde{p}_1 = |\tilde{e}_1|^2$, $\tilde{p}_2 = |\tilde{e}_2|^2$; the resulting equations take the form

$$\dot{e}_{1,2} = \tilde{e}_{1,2} - [1 + i(|e_{1,2}|^2 + 2|e_{2,1}|^2 - \Delta_{1,2})]e_{1,2}, \quad (10)$$

where the dot signifies the time derivative. Consequently, the theory shown in the first part of the paper – symmetry breaking and the sensitivity analysis – can be subsumed, as the steady state, within a time-dependent theory.

Stability analysis and oscillations.— Small perturbations of the electric field may grow or shrink with time. We investigate this by defining $e_1 = e_{s1} + \epsilon_1$ and $e_2 = e_{s2} + \epsilon_2$, where $\epsilon_{1,2}$ are small perturbations on the steady-state solutions, $e_{s1, s2}$. For simplicity, without loss of generality, we adjust the phases of $\tilde{e}_{1,2}$ such that $e_{s1, s2}$ are real. To characterise the time evolution of the resulting system of four equations, we form a 4×4 matrix, which has the following eigenvalues:

$$\lambda = -1 \pm \frac{\sqrt{-A_1 B_1 - A_2 B_2 \pm S}}{\sqrt{2}}, \quad (11)$$

$$S = \sqrt{(A_1 B_1 - A_2 B_2)^2 + 4A_1 A_2 C^2}, \quad (12)$$

in which $A_1 = e_{s1}^2 + 2e_{s2}^2 - \Delta_1$, $A_2 = 2e_{s1}^2 + e_{s2}^2 - \Delta_2$, $B_1 = 3e_{s1}^2 + 2e_{s2}^2 - \Delta_1$, $B_2 = 2e_{s1}^2 + 3e_{s2}^2 - \Delta_2$, and $C = 4e_{s1}e_{s2}$. The \pm signs are independent, giving four distinct eigenvalues. See Ref. [14] for more details. Qualitative changes in the eigenvalue describe transitions to different kinds of time-dependent behaviour: if λ is a

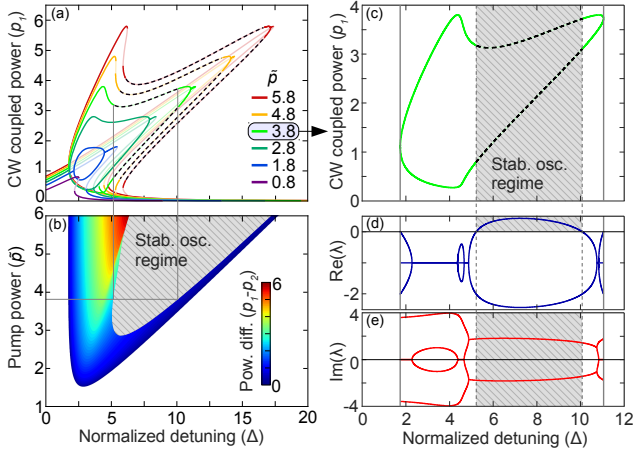


FIG. 4. Symmetry-broken solutions under balanced pumping. (a) Tilted resonances for various pump powers, showing the symmetry-broken region. Dark solid curves indicate stable solutions, faint curves show unstable solutions, and dashed curves correspond to oscillatory behaviour. (b) Amplitude of the difference in the coupled powers. The grey area corresponds to time-oscillating solutions (white denotes symmetric states). (c) Isolated curve for $\tilde{p} = 3.8$, from (a). (d) Real part of the stability eigenvalue, λ . (e) Imaginary part of the stability eigenvalue. Note that there always exists at least one eigenvalue with non-zero imaginary part, implying strong susceptibility to oscillations.

positive real number, the solution is a real, growing exponential, and the perturbed system will become unstable. Such unstable solutions occur for

$$(1 + X_1)(1 + X_2) < 4, \quad (13)$$

i.e., within the region enclosed by each of the curves in Fig. 3.

From Eq. (11) and the conditions of their existence, we have verified that it is not possible to have four real eigenvalues for the linear stability of the symmetry-broken solutions. This means that these solutions are strongly susceptible to either damped or sustained oscillations, since at least one stability eigenvalue is complex for experimentally relevant values of the parameters. Intuitively, oscillations are expected because of the simultaneous presence of two symmetry-broken solutions, under exchange of the indices (1, 2) in Eq. (10). In Fig. 4 (e) we show, for example, that for the chosen value of the pump $\tilde{p} = 3.8$, there is always at least one eigenvalue with non-zero imaginary part. In the case of negative real parts of the stability eigenvalues (between the vertical solid and dashed lines in Fig. 4 (c)–(e)) one observes damped oscillations where nonlinear resonances can be excited by suitable modulations of the pumps. When S in Eq. (12) is purely imaginary, we have four complex eigenvalues where the angular frequency, Ω , and the growth rate, R , are given respectively by

$$\Omega = \pm \sqrt{\frac{1}{2} \sqrt{A_1 A_2 (B_1 B_2 - C^2)} + \frac{1}{4} (A_1 B_1 + A_2 B_2)}, \quad (14)$$

$$R = -1 \pm \sqrt{\frac{1}{2} \sqrt{A_1 A_2 (B_1 B_2 - C^2)} - \frac{1}{4} (A_1 B_1 + A_2 B_2)}. \quad (15)$$

Here, again, the independent \pm signs give rise to four different complex solutions.

When R becomes positive, two Hopf bifurcations (forward and backward, when changing Δ) of the symmetry-broken solutions occur, allowing for non-decaying stable oscillations. We illustrate these oscillations as the dashed curves and shaded grey regions in Fig. 4. In frame (e) of this figure, we plot the corresponding frequencies of oscillation, Ω , from Eq. (14) when changing the detuning. We anticipate that this bifurcation will permit the construction of a microresonator-based all-optical oscillator, featuring periodic energy exchange between the two directions, in the nanosecond regime.

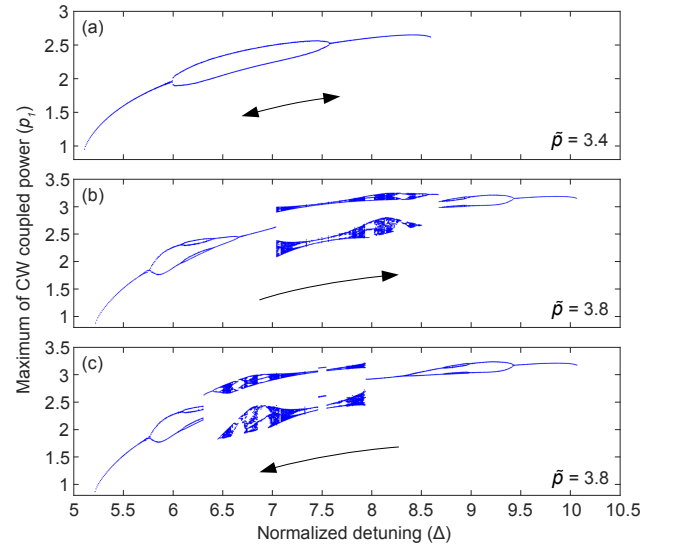


FIG. 5. Detuning scans of the oscillatory regimes of Eq. (10) between two Hopf bifurcations (lower solutions of Fig. 4 (a)). The field intensity is sampled at its maximum during the oscillation. The arrows indicate the direction of scanning the detuning. (a) Scan for $\tilde{p} = 3.4$ (showing no dependence on direction). Forward (b) and backward (c) scans for $\tilde{p} = 3.8$.

We have verified these predictions by direct numerical integration of Eq. (10). For each configuration specified by Δ and \tilde{p} , we have evaluated Poincaré sections when the intensity of one of the two fields (in our case $p_1 = |e_1|^2$) has a maximum given by the condition

$$p_i = |e_i|^2 = \tilde{e}_i \operatorname{Re}(e_i), \quad (16)$$

where $i = 1, 2$ and $\operatorname{Re}(e_i)$ is the real part of the complex field e_i , and we have now adjusted the phases such that

\tilde{e}_i is real. The Poincaré sections identify the oscillatory regimes and allow for dynamical scans when changing Δ . These scans are presented in Fig. 5 for $\tilde{p} = 3.4$, $\tilde{p} = 3.8$ while changing Δ from 5 to 11, and for $\tilde{p} = 3.8$ while changing Δ in reverse from 11 to 5. Each point in Fig. 5 corresponds to a nonlinear oscillation of the symmetry-broken output. The numerically-derived oscillation frequencies are in remarkably good agreement with those predicted by Eq. (14).

The forward and backward Hopf bifurcations are clearly visible at the beginning and the end of the scans. For values of input pumps just above the critical value of $\tilde{p} = 2.87$ where the Hopf bifurcations appear, regular oscillations occur at frequencies around four times the decay rate of the ring resonator, γ . We note that the point $(\tilde{p}, \Delta) = (2.87, 5.8)$ corresponds to a co-dimension 2 bifurcation where a forward and a backward Hopf bifurcations collide. Normal forms and unfoldings of double Hopf bifurcations provide the framework to establish the full dynamical behaviour of the symmetry-broken solutions [20]. In Fig. 5 (a) we show that forward and backward period doubling bifurcations occur close to the co-dimension 2 point ($\tilde{p} = 3.4$). By increasing the pump parameter, further period doubling bifurcations, deterministic chaos, collision of Feigenbaum cascades [21], and crises emerge, as shown in Fig. 5 (b) and (c) for $\tilde{p} = 3.8$. We observe bistable behaviour between these dynamical regimes, as shown in Fig. 5 (b) and (c), where the direction of the detuning scan is reversed.

Conclusion.—We have presented analytical and dynamical models for the interaction between counter-propagating light in a dielectric ring resonator. The mixture of self- and cross-phase modulation from the Kerr effect results in dramatic changes in behaviour: notably, spontaneous symmetry breaking and the onset of nonlinear oscillations – the latter holds promise for the development of highly controllable, on-chip, all-optical oscillators. We have also derived the universal condition for divergent sensitivity to perturbations, of which spontaneous symmetry breaking is a special case under balanced system conditions. This closed boundary of divergent sensitivity with respect to the laser detunings marks the transition between stable and unstable symmetry-broken solutions in a coupled, homogeneous system. The critical point lying on this boundary makes possible a variety of enhanced sensors for detecting rotations or near-field disturbances (e.g. biomolecules). In order to cover a wide range of experimental configurations, the scope of our analysis can be extended to systems featuring other forms of Kerr-nonlinearity-mediated symmetry breaking such as the interaction of light states of different polarisations, which would enable the development of optically controllable polarisation filters. In addition, this model is applicable to systems with different coefficients of self- and cross-phase modulation, such as semiconductors.

We acknowledge financial support from: H2020 Marie Skłodowska-Curie Actions (MSCA) (748519, CoLiDR); National Physical Laboratory Strategic Research; H2020 European Research Council (ERC)(756966, CounterLight); Engineering and Physical Sciences Research Council (EPSRC). L. H. acknowledges additional support from the EPSRC DTA Grant No. EP/M506643/1.

-
- [1] G. Baskaran & P. W. Anderson, ‘Gauge theory of high-temperature superconductors and strongly correlated Fermi systems’, *Phys. Rev. B*, **37**, 1 (1988).
 - [2] J. Bernstein, ‘Spontaneous symmetry breaking, gauge theories, the Higgs mechanism and all that’, *Rev. Mod. Phys.* **46**, 1 (1974).
 - [3] J. Rossi, R. Carretero-González, P. G. Kevrekidis & M. Haragus, ‘On the spontaneous time-reversal symmetry breaking in synchronously-pumped passive Kerr resonators’, *J. Phys. A: Math. Theor.* **49**, 45 (2016).
 - [4] B. Peng, Ş. K. Özdemir, F. Lei, F. Monifi, M. Gianfreda, G. L. Long, S. Fan, F. Nori, C. M. Bender & L. Yang, ‘Nonreciprocal light transmission in parity-time-symmetric whispering-gallery microcavities’, *Nat. Phys.* **10**, 394 (2014).
 - [5] F. Copie, M. T. M. Woodley, L. Del Bino, J. M. Silver, S. Zhang & P. Del’Haye, ‘Interplay of Polarization and Time-Reversal Symmetry Breaking in Synchronously Pumped Ring Resonators’, arXiv:1807.02347 (2018).
 - [6] L. Del Bino, J. M. Silver, S. L. Stebbings & P. Del’Haye, ‘Symmetry Breaking of Counter-Propagating Light in a Nonlinear Microresonator’, *Sci. Rep.* **7**, 43142 (2017).
 - [7] Q.-T. Cao, H. Wang, C.-H. Dong, H. Jing, R.-S. Liu, X. Chen, L. Ge, Q. Gong & Y.-F. Xiao, ‘Experimental demonstration of spontaneous chirality in a nonlinear microresonator’, *Phys. Rev. Lett.* **118**, 033901 (2017).
 - [8] A. E. Kaplan & P. Meystre, ‘Enhancement of the Sagnac Effect due to nonlinearly induced nonreciprocity’, *Opt. Lett.* **6**, 12 (1981).
 - [9] A. E. Kaplan & P. Meystre, ‘Directionally asymmetrical bistability in a symmetrically pumped nonlinear ring interferometer’, *Opt. Commun.* **40**, 3 (1982).
 - [10] L. Del Bino, J. M. Silver, M. T. M. Woodley, S. L. Stebbings, X. Zhao & P. Del’Haye, ‘Microresonator isolators and circulators based on the intrinsic nonreciprocity of the Kerr effect’, *Optica* **5**, 3 (2018).
 - [11] Q.-F. Yang, X. Yi & K. Vahala, ‘Counter-propagating solitons in microresonators’, *Nat. Photonics* **11** 560-564 (2017).
 - [12] P. Trocha, M. Karpov, D. Ganin, M. H. P. Pfeiffer, A. Kordts, S. Wolf, J. Krockenberger, P. Marin-Palomo, C. Weimann, S. Randel, W. Freude, T. J. Kippenberg & C. Koos, ‘Ultrafast optical ranging using microresonator soliton frequency combs’, *Science* **359**, 6378 (2018).
 - [13] M.-G. Suh & K. J. Vahala, ‘Soliton microcomb range measurement’, *Science* **359**, 6378 (2018).
 - [14] Supplemental Material at [URL link].
 - [15] C. Godey, ‘A bifurcation analysis for the Lugiato Lefever equation’, *Eur. Phys. J. D* **71**, 131 (2017).
 - [16] M. Haelterman, S. Trillo & S. Wabnitz, ‘Polarization multistability and instability in a nonlinear dispersive

- ring cavity', *J. Opt. Soc. Am. B* **11**, 3 (1994).
- [17] J. B. Geddes, J. V. Moloney, E. M. Wright & W. J. Firth, 'Polarisation patterns in a nonlinear cavity', *Opt. Commun.* **111**, 623-631 (1994).
- [18] X. Jiang, A. J. Qavi, S. H. Huang & L. Yang, 'Whispering gallery microsensors: a review', arXiv:1805.00062 (2018).
- [19] M. R. Foreman, J. D. Swaim & F. Vollmer, 'Whispering gallery mode sensors', *Adv. Opt. Photon* **7**, 2 (2015).
- [20] E. Knobloch & M. R. E. Proctor, 'The double Hopf bifurcation with 2:1 resonance', *Proc. R. Soc. Lond. A* **415**, 61-90 (1988).
- [21] G.-L. Oppo & A. Politi, 'Collision of Feigenbaum cascades', *Phys. Rev. A* **30**, 435-441 (1984).